SUPPLEMENTARY INFORMATION

1. ElectroDeposition Template Fabrication

The fabrication of the electrode/template for ED started with a 100 mm diameter n-type silicon wafer (Fig. S1.a). A 200 nm thick silicon dioxide layer was thermally grown using a wet oxidation procedure at 1100°C (Fig. S1.b). EBL step was then performed on the wafer using ZEP as the resist. In this step, arrays of holes are defined inside the resist together with two big openings for posterior electrical contacts needed for ED. After development (Fig. S1.c), a combination of dry and wet etching processes was used to transfer the nanopatterns from the resist to the oxide. First, a dry etch (C_2F_6, 200 sccm, 2000 W source power, 400 W platen power) was performed to etch most of the layer (approx. 180 nm), followed by a thorough oxygen plasma in order to clean the wafer from any possible polymeric residues. The remaining 20 nm of SiO_2 were etched in a buffered solution of Hydrofluoric acid (BHF) for 15 seconds (Fig. S1.d). This final step was taken to ensure proper contact of the n-type silicon surface with the platting solution during the subsequent ED. Immediately prior to ED, an additional oxide etching (in order to remove native oxide that grows naturally on Si surface) was performed with HF (10% vol) for 30 seconds, followed by a thorough rinsing using ultrapure water (18 MΩ) for 5 minutes.

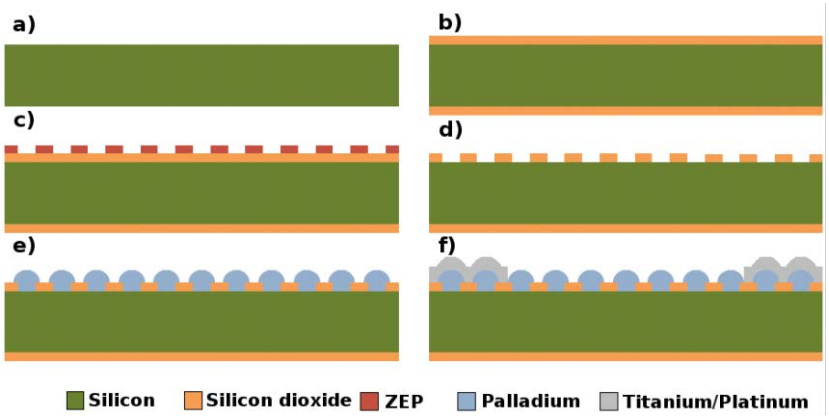

Figure S1. Process flow for the fabrication of ED electrode/templates. (a) n-type silicon wafer (100 mm in diameter). (b) 200 nm thick layer of silicon dioxide is thermally grown. (c) e-beam lithography is performed using ZEP as a resist. (d) Patterns transfer using a combination of dry and wet etch processes. (e) ED of Pd. (f) Contact electrodes (10 nm Ti/100 nm Pt) deposition by stencil mask evaporation.

Some typical results of electrodeposition templates obtained by the method just described can be found in Figure S2, with examples of square and hexagonal networks and square-shaped and circular-shaped individual templates.

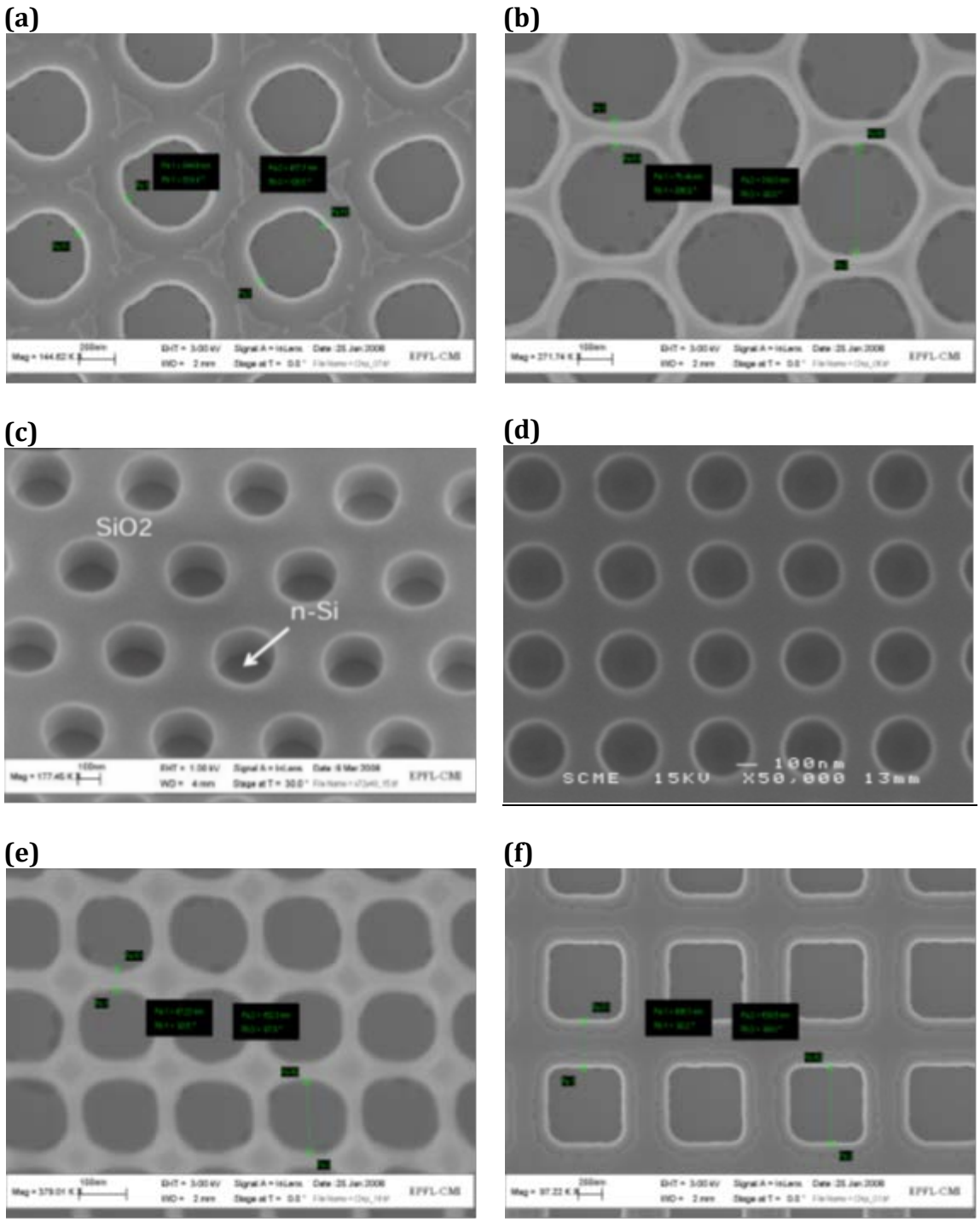

Figure S2. SEM micrographs showing various electrode/template designs. (a-b) hexagonal 3D arrangement, (c-f) square 2D arrangement. (a-d) Circular individual holes, (e-f) squared individual holes. These micrographs show a small part of the spectrum of different hole depths, diameter and inter-hole distance (or wall thickness) that were tried during fabrication.

2. Pd ElectroDeposition

For ED, templates were contacted using stainless-steel tweezers. All the platting solutions used for this work were based on PdCl2 dissolved in HCl supporting electrolyte (5mM Pd2+ in 0.1M HCl). Template electrodes were set as working electrode in a conventional 3-electrode setup (Ag-AgCl reference electrode and Pt foil as counter electrode). Single step electrolyses were performed in galvanostatic mode at various currents ranging from -50 µA to -500 µA. Electrolysis charges were controlled and limited to -50 mC to -250 mC as charge appeared as a critical parameter for the ED reproducibility and preparation of calibrated deposits. At the corresponding potentials (-0.1 to -0.8 V/AgAgCl), Pd^{2+} ions from the platting solution were reduced allowing Pd to nucleate at the open surface of the n-doped silicon inside the holes of the patterned insulating SiO2 layer. From these nuclei, Pd started to grow as disordered nanoparticle aggregates within the hole vicinity (Figure S3.a) before to overgrow as hemispherical polycrystalline deposits accros the surface of the silica layer. (Fig. S1.e). The size of the deposits was controlled by the ED duration. The electrodeposition process was stopped before contact between neighboring Pd deposits occurs to obtain a well ordered 2D array of isolated palladium dots. After the ED was finished, a metallic bi-layer of titanium/platinum (10 nm/100 nm) was deposited via shadow mask evaporation for contact electrodes fabrication (Fig. S1.f).

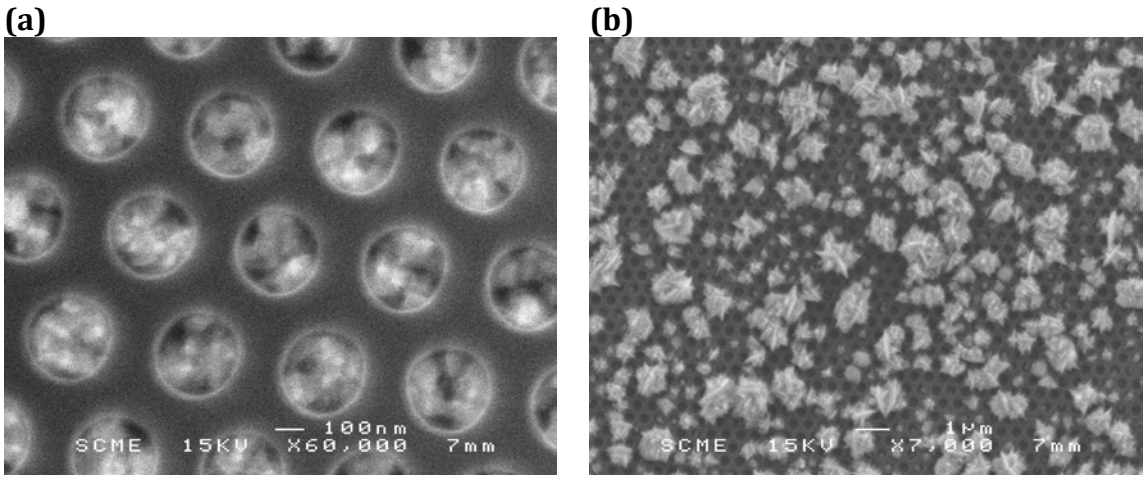

Figure S3. SEM micrographs showing different ED results. (a) Template surface after Pd ED for 4min at -50µA (before overgrowth) confirming the polycrystalline nature of the Pd deposits. (b) Heterogeneous (undesirable) ED of Pd leading to empty holes together with large deposits merging several neighbor dots.

3. Sensor response curve

The response of this type of sensors is observed by monitoring the current that they allow at a given fixed voltage. The relative change in current (or in conductivity) remains reproducible. In Figure S4, the reproducibility of the relative change in conductivity can be observed, showing 10 consecutive hydrogen exposures of a given sensor. The increase of the lowest point in conductance is due to an incomplete hydrogen desorption, which also explains why the drift in the "off" state asymptotically reduces as the H2 concentration decreases.

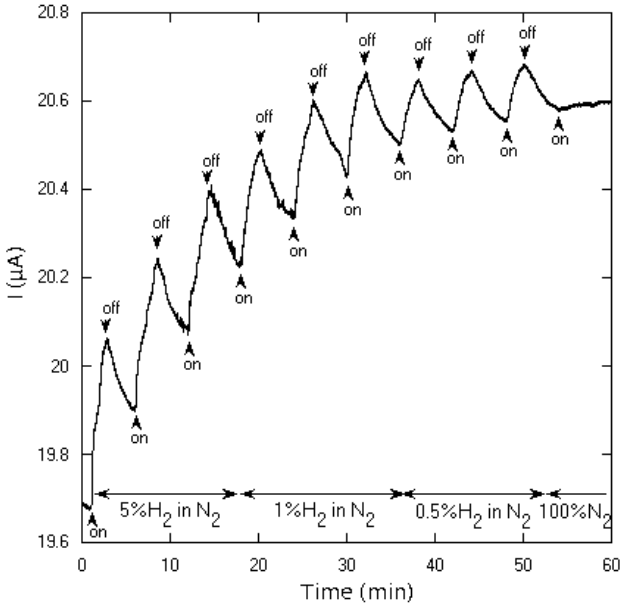

Figure S4. Sensor response curve. Current response of a sensor under various H2 in N2 atmospheres demonstrating the repeatability of the sensor response. Under pure N2, the sensor shows no response. Flow rate 20 mL/min. In off state, hydrogenated flow is switch off and the sensor is left at open air.

4. AFM observation of Pd expansion during H2 exposure

Figure S5 shows a SEM micrograph (Figure S5a) and Atomic Force Microscopy (AFM) topographic images of the exact same spot at the sensor surface in air (Figure S5b) and under a stream of pure hydrogen gas (Figure S5c). In this picture series, image features are so different that the dot shape imaged by SEM is hardly recognizable on AFM topographic images. The dot roughness is better shown by AFM imaging relaying on the dot topological characteristics while surface details are obviously flattened by SEM because of the limited electronic contrast in such pure palladium deposits. A close look to these images confirms that the surface of the dots is composed of faceted grains and dendrites of various sizes and orientations, accounting for a wide distribution in the dot size separation. As an example, a selection of nanogaps is highlighted and numbered (#1 to #5) on the AFM image taken in air (Figure S5b) with sizes ranging from 61nm to 30nm. Corresponding break junctions are numbered the same way on the AFM image taken under H2 (Figure S5c). The topography profiles (Figure S5d) of the selected nanogaps are shown to decrease. The same trend can be observed for all of them as summarized in the table included in Figure S5 with decreases up to 35% from the initial gap size in air.

None of the selected nanogaps actually closed under H2. It is indeed very challenging to find such nanogaps due to the fact that it is very difficult to experimentally measure with the AFM a gap that is small enough that can be spotted in air while closing under H2 (tip-convolution problem).

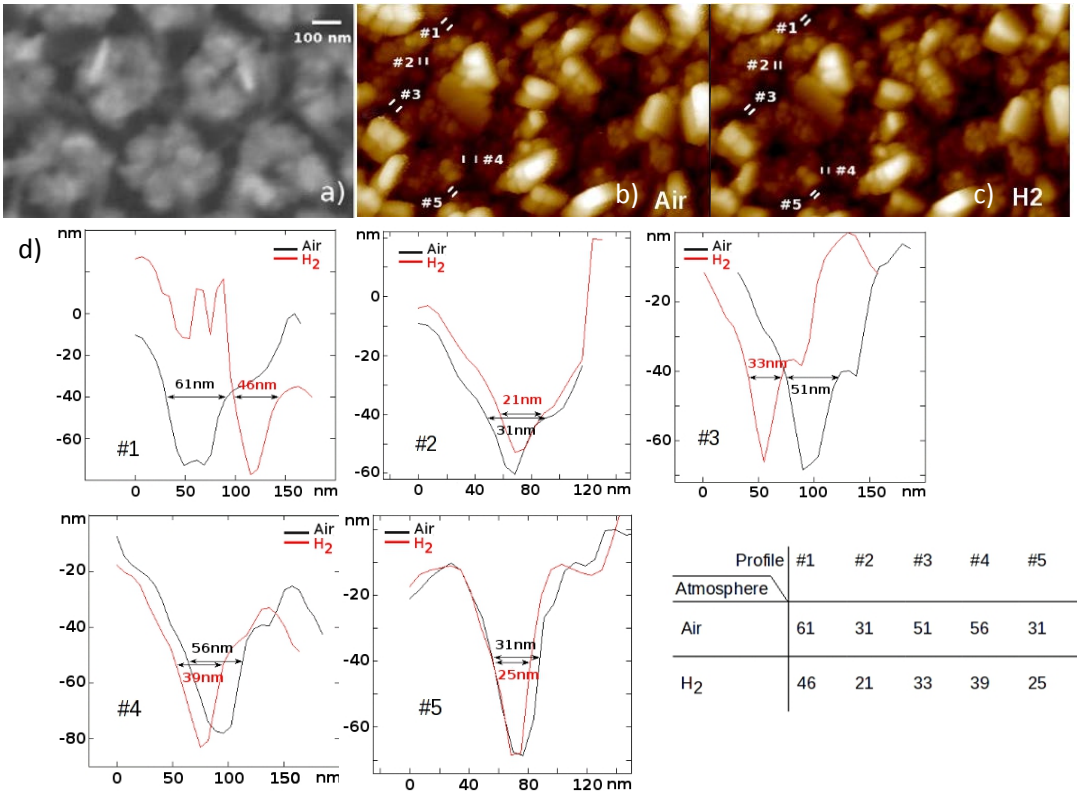

Profile / Atmosphere	#1	#2	#3	#4	#5
Air	61	31	51	56	31
H_2	46	21	33	39	25

Figure S5. Sensing mechanism explored by AFM. 1200x700nm^2 micrographs of the sensor surface were taken at the exact same spot. (a) SEM image of electrodeposited palladium dots, (b) and (c) AFM corresponding images. Image (b) was acquired in air; image (c) was acquired in a stream of pure hydrogen gas. A series of hydrogen-actuated nanogaps are highlighted (#1 to #5). (d) Topographical plots of all selected nanogaps along the short span direction showing the narrowing of the break junction under H2. The table summarizes the span distances (nm) in air and under H2 for the selected nanogaps.